

Sinusoidal voltage protocols for rapid characterisation of ion channel kinetics

Kylie A. Beattie^{1,2}, Adam P. Hill^{3,4}, Rémi Bardenet⁵, Yi Cui⁶, Jamie I. Vandenberg^{3,4},
David J. Gavaghan¹, Teun P. de Boer⁷, Gary R. Mirams⁸

January 31, 2018

1. Computational Biology, Department of Computer Science, University of Oxford, OX1 3QD, UK.
2. Division of Applied Regulatory Science, Office of Clinical Pharmacology, Office of Translational Sciences, Center for Drug Evaluation and Research, Food and Drug Administration, Silver Spring, MD, USA.
3. Department of Molecular Cardiology and Biophysics, Victor Chang Cardiac Research Institute, Sydney, NSW 2010, Australia.
4. St Vincent's Clinical School, UNSW Sydney, Darlinghurst, NSW 2010, Australia.
5. CNRS & CRISAL, Université de Lille, 59651 Villeneuve d'Ascq, France.
6. Safety Evaluation and Risk Management, Global Clinical Safety and Pharmacovigilance, GlaxoSmithKline, Uxbridge, UB11 1BS, UK.
7. Department of Medical Physiology, Division of Heart & Lungs, University Medical Center Utrecht, Utrecht, The Netherlands.
8. Centre for Mathematical Medicine & Biology, School of Mathematical Sciences, University of Nottingham, NG7 2RD, UK.

Running Title: Sinusoidal protocols to capture ion channel kinetics

Corresponding Author: Gary Mirams <gary.mirams@nottingham.ac.uk>

Mathematical Sciences,
University Park,
Nottingham,
NG7 2RD,
United Kingdom.

Table of Contents Category: Techniques for Physiology¹

¹This article was first published as a preprint on bioRxiv: Beattie *et al.* (2017): <https://doi.org/10.1101/100677>

1 Key Points

- 2 • Ion current kinetics are commonly represented by current-voltage relationships, time-constant
3 voltage relationships, and subsequently mathematical models fitted to these. These experi-
4 ments take substantial time which means they are rarely performed in the same cell.
- 5 • Rather than traditional square-wave voltage clamps, we fit a model to the current evoked by
6 a novel sum-of-sinusoids voltage clamp that is only 8 seconds long.
- 7 • Short protocols that can be performed multiple times within a single cell will offer many new
8 opportunities to measure how ion current kinetics are affected by changing conditions.
- 9 • The new model predicts the current under traditional square-wave protocols well, with bet-
10 ter predictions of underlying currents than literature models. The current under a novel
11 physiologically-relevant series of action potential clamps is predicted extremely well.
- 12 • The short sinusoidal protocols allow a model to be fully fitted to individual cells, allowing us
13 to examine cell-cell variability in current kinetics for the first time.

14 Abstract

15 Understanding the roles of ion currents is crucial to predict the action of pharmaceuticals
16 and mutations in different scenarios, and thereby to guide clinical interventions in the heart,
17 brain and other electrophysiological systems. Our ability to predict how ion currents contribute
18 to cellular electrophysiology is in turn critically dependent on our characterisation of ion chan-
19 nel kinetics — the voltage-dependent rates of transition between open, closed and inactivated
20 channel states. We present a new method for rapidly exploring and characterising ion channel
21 kinetics, applying it to the hERG potassium channel as an example, with the aim of generat-
22 ing a quantitatively predictive representation of the ion current. We fit a mathematical model
23 to currents evoked by a novel 8 second sinusoidal voltage clamp in CHO cells over-expressing
24 hERG1a. The model is then used to predict over 5 minutes of recordings in the same cell in
25 response to further protocols: a series of traditional square step voltage clamps, and also a novel
26 voltage clamp comprised of a collection of physiologically-relevant action potentials. We demon-
27 strate that we can make predictive cell-specific models that outperform the use of averaged data
28 from a number of different cells, and thereby examine which changes in gating are responsible
29 for cell-cell variability in current kinetics. Our technique allows rapid collection of consistent
30 and high quality data, from single cells, and produces more predictive mathematical ion channel
31 models than traditional approaches.

32
33 **Keywords:** hERG, I_{Kr} , mathematical model, electrophysiology, patch clamp, voltage proto-
34 col

35 Non-standard Abbreviations and Acronyms

- 36 • CHO — Chinese Hamster Ovary [cells].
- 37 • G_{Kr} — maximal conductance of I_{Kr} .
- 38 • HEK — Human Embryonic Kidney [cells].
- 39 • hERG — human Ether-a-go-go Related Gene.
- 40 • I_{Kr} — rapid delayed rectifying potassium current, carried by the $K_v11.1$ ion channel whose
41 primary subunit is encoded by hERG.

42 1 Introduction

43 Mathematical models of ion channels are a quantitative expression of our understanding of ion
44 channel kinetics: they express the probability of channels existing in different conformational states
45 (typically, closed, open and inactivated) and the rates of transition between these states (Bett
46 et al., 2011; Vandenberg et al., 2012). Parameterising/calibrating a mathematical model of an
47 ion current is a concise way to characterise ion channel kinetics, to capture our understanding
48 in a quantitative framework, and to communicate this knowledge to others. There have been
49 some notable advances in deriving mathematical models for ion channel behaviour (Balsler et al.,
50 1990; Cannon and D’Alessandro, 2006; Siekmann et al., 2011, 2012; Loewe et al., 2015), with some
51 stressing the need for validation/testing of the model using data from the same cell (Tomaiuolo et
52 al., 2012). In this paper we present a new approach for characterising ion channel kinetics, using
53 novel short protocols and parameter inference techniques to construct an ion channel model.

54 The *KCNH2* gene (also known as *hERG*) has been shown to encode the primary subunit of
55 the voltage-gated ion channel Kv11.1 that carries the rapid delayed rectifier potassium current
56 (I_{Kr}) (Trudeau et al., 1995; Sanguinetti et al., 1995). In this article we focus on mathematical
57 modelling of hERG channel kinetics, demonstrating our approach by constructing an improved
58 model of this ion current. hERG plays important roles in the brain (Babcock and Li, 2013);
59 gastrointestinal tract (Farrelly et al., 2003); uterine contractions (Parkington et al., 2014); cell-
60 proliferation and apoptosis (Jehle et al., 2011) and cancer progression (Lastraioli et al., 2015), but
61 I_{Kr} is best known as a repolarising cardiac ion current. The channel is susceptible to binding and
62 blockade by pharmaceutical compounds, which is strongly linked to many cases of drug-induced
63 pro-arrhythmic risk (Redfern et al., 2003; Pollard et al., 2010). Mathematical modelling of cardiac
64 electrophysiology, including I_{Kr} , forms a core part of a new proposal for routine *in vitro* and *in*
65 *silico* safety assessment to replace a human clinical drug safety study (Sager et al., 2014; Fermini
66 et al., 2016). A wide range of different mathematical models have been proposed to describe I_{Kr}
67 (literature models are listed in Appendix A, Table A1).

68 Fig 1 shows predicted I_{Kr} under three different voltage clamps for 29 literature models. These
69 models were developed to describe different species, cell types, temperatures and isoforms, so vari-
70 ation is expected. In Figure 1B–E each row highlights models developed to represent the same
71 species, cell type and temperature; even models for the same conditions provide highly variable
72 predictions.

73 The first models of ion channel kinetics were proposed by Hodgkin and Huxley (1952), and
74 relatively little has changed in the methods used for construction of mathematical models of ion
75 channel gating since the original seminal work in this journal in 1952. Their (now traditional)
76 approach is to fit peak currents and time constants of current activation/decay after clamping to
77 fixed voltages; to assemble current/voltage (IV) and time-constant/voltage (τ -V) curves; and to
78 describe these curves with interpolating functions.

79 Condensed voltage clamp step protocols have been suggested as the basis of optimised experi-
80 ments that provide information about ion channel kinetics faster than experiments to construct IV
81 curves (Hobbs and Hooper, 2008; Fink and Noble, 2009); and optimised current and square step
82 voltage clamps have been used to optimise the fitting of maximal conductances in action poten-
83 tial models (Groenendaal et al., 2015). Single sinusoid voltage clamps have been previously been
84 explored for choosing between possible Shaker channel models that were parameterised using tradi-
85 tional square step voltage clamps (Kargol et al., 2004). Wavelet-based voltage protocols have also
86 been suggested for examining sodium channel dynamics (Hosein-Sooklall and Kargol, 2002). The
87 study by Kargol (2013) features excellent insight into the problem of models behaving similarly
88 under traditional clamps but differently under optimised information-rich protocols. In that paper,

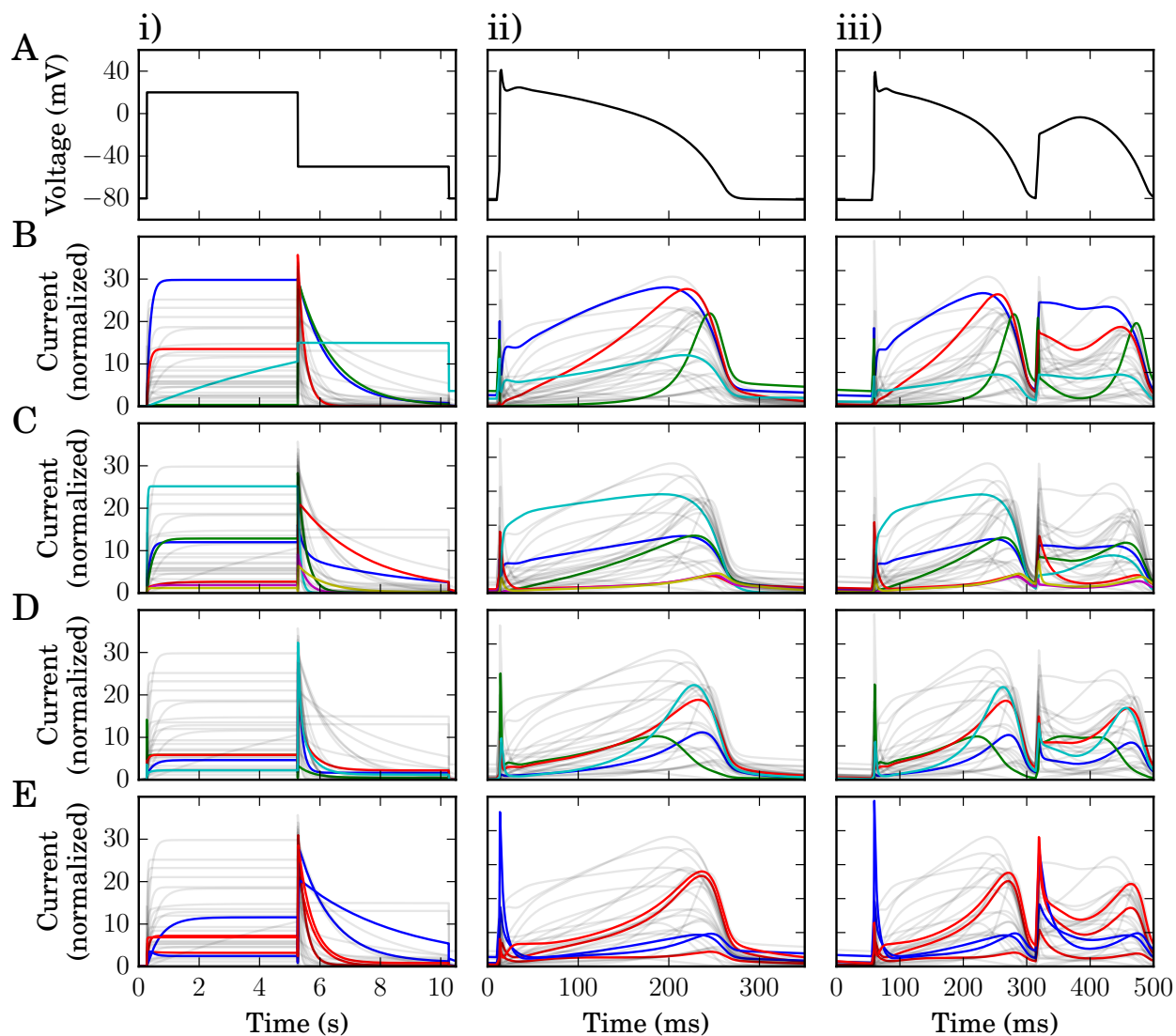


Figure 1: **Current predictions from literature models of I_{K_r} .** Each column shows simulated current predictions from 29 I_{K_r} literature models in response to the different voltage clamp protocols shown in the top row. **(A)** voltage clamps: i) a voltage-step; ii) an action potential; and iii) an action potential displaying pathological properties. Each of the panels below features all 29 current predictions in faint grey, to aid comparison between plots. **(B)** In row B we highlight the four models for canine ventricle at physiological temperature. **(C)** In row C we highlight the six models for human ventricle at physiological temperature. **(D)** In row D we highlight the four models for rabbit sino-atrial node at physiological temperature. **(E)** In row E we highlight the five models for hERG1a expression systems: at room temperature in blue; and physiological temperature in red. Currents are normalised such that the maximal conductance is equal to one; i.e. we plot the open probability multiplied by the driving voltage (all model references and structures are listed in Table A1 in Appendix A). All models have been simulated with their original published parameters, with the same reversal potential of -88.4 mV.

89 these wavelet-based protocols were designed and used to select between Shaker potassium channel
90 models.

91 In this study, we extend these ideas and propose an 8 second sum-of-sinusoids-based voltage
92 clamp, designed to both explore and fully-characterise the kinetics of the hERG potassium channel.
93 We use this new protocol to record currents from Chinese Hamster Ovary (CHO) cells that are
94 over-expressing hERG1a. These recordings are then used to parameterise a mathematical model
95 which becomes our characterisation of the ion current. We then evaluate the model by predicting
96 the response to both standard square step voltage-clamp protocols and perhaps more importantly
97 physiologically-relevant action potential voltage clamps: using these data (which are independent of
98 the recordings used to fit the model) to perform an extremely thorough validation for the model of
99 ion channel kinetics. Our approach uses a substantially shorter experimental recording to construct
100 the model than the usual approach, which is based on time constants and peak currents from a long
101 series of square step voltage-clamp protocols. As a consequence of the high information content of
102 the short protocol, we are able to generate cell-specific models that advance our understanding of
103 variability of ion currents between cells. Our methodology will be applicable to many ion channels,
104 both in the heart and other electrophysiological systems.

105 2 Methods

106 2.1 Experimental methods

107 We performed whole-cell patch-clamp voltage clamp experiments, using CHO cells stably expressing
108 hERG1a (Kv11.1) at room temperature. Full details including cell culture, solutions, and equipment
109 settings can be found in Appendix B. In Figure 2 we provide an overview of the experimental
110 approach, denoting the sequence of voltage clamp protocols we performed as Pr0–Pr7.

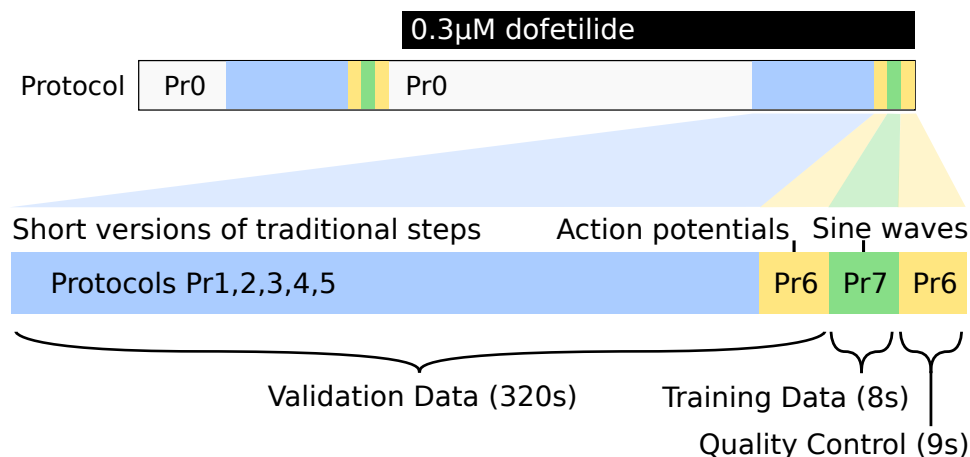


Figure 2: **Schematic diagram of the experimental procedure used in this study** (not to scale). A simple activation step protocol is repeated in the sections marked ‘Pr0’, before moving on to the highlighted section (below) where data used in the study were recorded. The recording protocols ‘Pr1–7’ are performed twice, once before dofetilide addition, and once after, with the hERG current isolated by subtraction. For full details of the protocols please refer to Appendix B1.4.

111 In each cell we recorded: a series of conventional voltage-step protocols designed to explore
112 activation (Pr1–3), inactivation (Pr4) and deactivation (Pr5); a new protocol composed of a series
113 of action potential clamps (Pr6 — formed of simulated action potentials from different mathematical

114 models to represent diverse species and pacing frequencies in both healthy and repolarisation-failure
115 conditions); and our new 8 s sinusoidal voltage protocol (Pr7, shown in Figure 3). These protocols
116 are all performed in a single experiment using a single cell, and the process can be repeated in
117 different cells. A mathematical model is then fitted/calibrated to solely the current provoked by the
118 sinusoidal protocol, and this model then represents a full characterisation of I_{K_r} in each particular
119 cell. The characterisation is then tested for accuracy by using the fitted mathematical model to
120 predict the results of all the other voltage clamp protocols performed in that cell. Full details of all
121 protocols are given in Appendix B1.4.

122 In all protocols, the holding potential was initially -80 mV before applying a 50 ms leak step to
123 -120 mV before returning back to -80 mV, with this step being used to estimate leak current (as
124 described below in Section 2.2). A voltage step to -120 mV at the end of all the protocols ensures
125 that channels close quickly, reducing the time needed between protocols to regain a steady closed
126 state.

127 **Protocols 0 to 5 — Square Step Clamps**

128 Protocol 0 is a simple repeated activation pulse designed to open the channel to visually test the
129 recordings were stable and to allow dofetilide binding, considered open state dependent, to occur
130 (see Section 2.3, below). This current was not recorded or used in the subsequent analysis (hence
131 ‘Protocol 0’).

132 Protocols 1–5 are adaptations of ‘traditional’ square step voltage clamps used in previous studies
133 to examine activation (Pr1–3), inactivation (Pr4) and deactivation (Pr5). Details of the protocol
134 voltages and timings can be found in Appendix B1.4.

135 The ‘adaptation’ is that protocols 1–5 are shorter than those previously used to calibrate math-
136 ematical models (as in fewer test voltages/timings are used), so that it is possible to perform them
137 all in a single cell, with and without dofetilide subtraction. A ‘traditional approach’ would take
138 longer than the experiments performed here, generally requiring multiple cells.

139 **Protocol 6 — Action Potentials Clamp**

140 This protocol was formed by combining a series of different simulated action potentials from the
141 Cardiac Electrophysiology Web Lab (Cooper et al., 2016). The range of models we used for the
142 simulations encompassed different cell types, species, and pacing rates. We also added some sim-
143 ulated action potentials where early or delayed after-depolarisations had been induced, to test I_{K_r}
144 behaviour in pro-arrhythmic or pathological settings. The action potentials were shifted slightly so
145 that their resting potentials were exactly -80 mV (see the Supplementary Code for full details and
146 code to reproduce this protocol).

147 **Protocol 7 — Sinusoidal Clamp**

148 The protocol used to characterise the current and train the model is a voltage clamp comprised of
149 simple steps and a main sinusoidal section that is in the form of a sum of three sine waves of different
150 amplitudes and frequencies, designed to rapidly explore hERG channel kinetics. The underlying
151 rationale is to force the protocol to ‘sweep’ both the time and voltage dependence of the current
152 gating over physiological voltage ranges.

153 The start of the protocol takes the form of a leak step followed by a simple activation step which
154 is similar to Protocol 0. This activation step was included to improve the identifiability of the
155 maximal conductance parameter (as described in Appendix B2.2) after preliminary experiments
156 suggested this might improve what is known as ‘parameter identifiability’ (to pin down possible

157 values of the parameter more accurately, and prevent other kinetic parameters compensating for an
158 inaccurate conductance value).

159 The main sinusoidal portion of the protocol takes the form of a sum of three sine waves as shown
160 in Equation (1):

$$V(t) = -30 + A_1 \sin(\omega_1(t - t_0)) + A_2 \sin(\omega_2(t - t_0)) + A_3 \sin(\omega_3(t - t_0)), \quad (1)$$

161 where $A_1 = 54$ mV, $A_2 = 26$ mV, $A_3 = 10$ mV, $\omega_1 = 0.007$ ms⁻¹, $\omega_2 = 0.037$ ms⁻¹ and $\omega_3 =$
162 0.19 ms⁻¹, and t is time measured in milliseconds.

163 In terms of frequencies, existing models and I_{K_r} recordings include characteristic timescales of
164 order 10 ms to one second (Wang et al., 1997; Zhou et al., 1998). Therefore we designed the sinusoidal
165 protocol's three frequencies to probe channel kinetics across all these orders of magnitude (10 ms,
166 100 ms and 1 s timescales). We selected frequencies that were co-prime rather than exactly multiples
167 of ten: ω_1 to ω_3 are ordered slow to fast and correspond approximately to sine waves of period 900,
168 170 and 33 ms, respectively. The aim was that the three distinct frequencies should not become
169 'in phase': the protocol never repeats patterns that the cell has experienced before (ensuring new
170 information is supplied throughout). The offset t_0 is 2500 ms as explained in Appendix B1.4. If
171 one was to study other ion channels, these frequencies may need adjustment to examine relevant
172 timescales.

173 To decide the amplitudes, the oscillations are centred around -30 mV so that a physiological
174 range is explored ($-120 < V < 60$ mV). The amplitudes of the sine waves were selected to keep
175 the protocol within this range ($A_1 + A_2 + A_3 = 90$ mV) and to ensure that $A_1 > A_2 > A_3$ so that
176 the fastest timescale had the smallest oscillations (to avoid the faster gating processes masking the
177 voltage-dependence of slower ones).

178 A key step in settling on this particular protocol was its performance in *synthetic data* studies.
179 In these studies we simulated I_{K_r} with different sets of given parameters, then attempted to recover
180 these parameters blindly — using just the generated current trace with added noise, as illustrated
181 in Appendix C2 (we also show this for an I_{K_s} model with the same protocol in Appendix G).

182 The sinusoidal protocol is of only eight seconds duration, which enables efficient data collection,
183 with training and validation data collected from the same cell. In Figure 3 we present the novel
184 sinusoidal protocol Pr7, the simulated predicted currents from existing models, and the currents we
185 recorded experimentally. The new protocol provokes an even wider array of different behaviours
186 from the existing literature I_{K_r} models (middle panels in Figure 3) than the existing voltage step or
187 action potential clamps (Figure 1); even among models constructed in/for similar conditions/species.

188 2.2 Leak Corrections

189 We used the leak-step from -80 mV to -120 mV in order to leak-correct the experimental data,
190 according to:

$$I_{\text{corrected}} = I_{\text{raw}} - V/R_{\text{leak}}. \quad (2)$$

191 We identified the most appropriate R_{leak} value to minimise the difference between the mean current
192 value during the leak step (to -120 mV) compared to the mean value at a holding potential of
193 -80 mV, whilst ensuring that the trace was not over-corrected (which would result in negative
194 currents during the initial stages of activation).

195 We manually selected leak resistances to correct the current evoked by the sinusoidal protocol
196 in both vehicle and dofetilide conditions. We then applied this leak resistance to the remaining
197 protocols performed in the same condition on each cell.

198 The mean current during the -80 mV step was calculated from 200 ms of the -80 mV holding
199 period before the -120 mV leak step (not including the capacitive spike at the point at which the

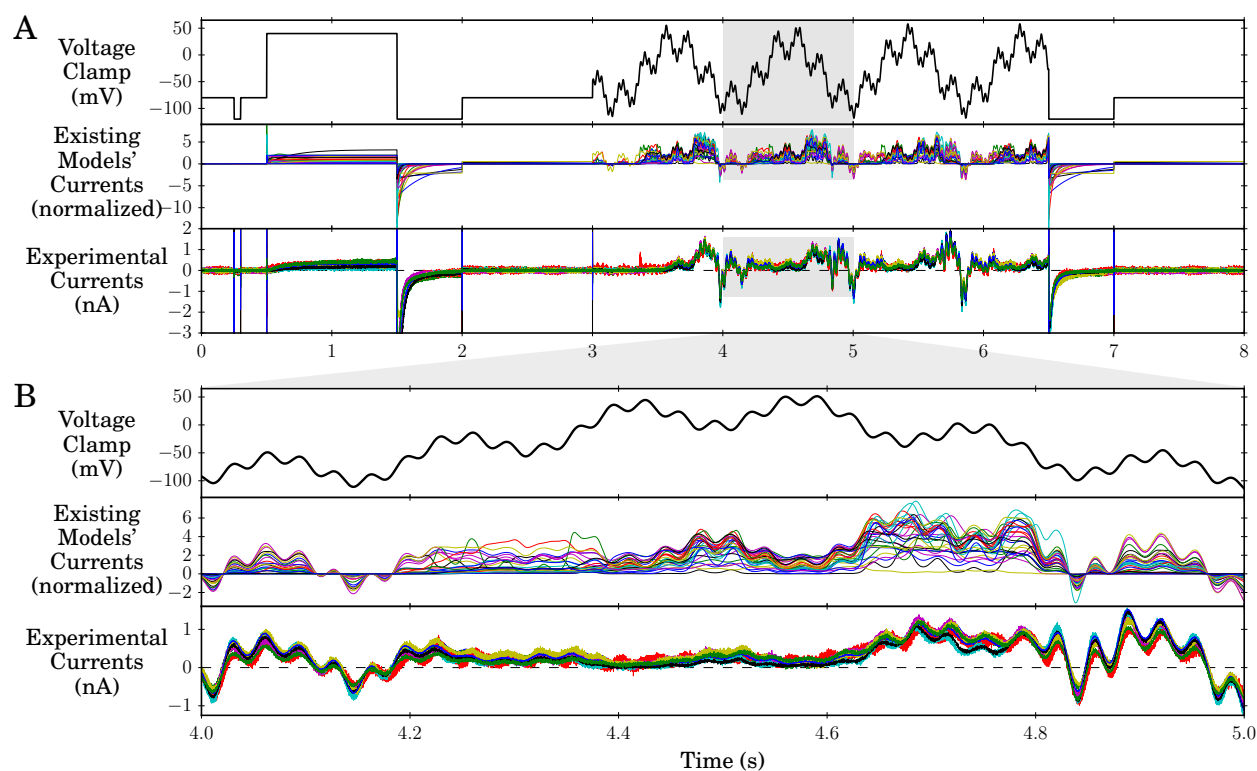


Figure 3: **The sinusoidal protocol and example recordings.** **A: Top row:** The full sinusoidal voltage protocol (Pr7). **Middle row:** Simulations of expected behaviour in response to this protocol from existing I_{K_r} and hERG models, normalised by scaling the conductance value for each model to minimise the absolute difference between each trace and a reference trace. For calculation of the reversal potential, a temperature of 21.5 °C was used to match the mean experimental conditions. **Bottom row:** Raw data (following leak and dofetilide subtraction) from experimental repeats at room temperature from 9 cells. Experimental traces have been scaled, to remove the effect of different maximal conductances, by a factor chosen to minimise the absolute differences between each trace and a reference experimental trace (that with the peak current during the sinusoidal portion of Pr7). **B:** an enlargement of the highlighted sections of panel A. Whilst there is some variation between cells in the experimental results, they are much more consistent than the predictions from the different models.

200 step occurs). The baseline current at a holding potential of -80 mV was then adjusted back to 0 nA
201 with an additional constant additive current if required.

202 2.3 Dofetilide Subtraction

203 In preliminary work, we observed that our sinusoidal protocols could elicit endogenous voltage-
204 dependent background currents within expression-system cells. We observed that the levels of
205 endogenous currents the protocols elicited varied from cell to cell. These currents could adversely
206 affect the predictive ability of the resulting mathematical models, as the fitting process attempted
207 to create a model that described both the endogenous and I_{K_r} components of the recorded currents.
208 To overcome this technical issue we made a number of alterations to our pilot experiments.

209 Firstly, we constrained the design of the sinusoidal protocol, as discussed above, so that only
210 voltages within a physiological range of -120 mV to $+60$ mV were explored, as endogenous currents

211 were much more prominent at voltages above +60 mV that we explored in pilot studies.

212 Secondly, we changed to use CHO cells in this study, rather than the HEK cells we used in pilot
213 studies, as CHO cells generally had lower endogenous currents.

214 Thirdly, we recorded the full set of voltage protocols (Pr1–7) twice: once in Dimethyl sulfoxide
215 (DMSO) vehicle conditions and once following the addition of 0.3 μM dofetilide, as shown in Figure 2.
216 Dofetilide was first dissolved in DMSO before being added to the bath solution to produce the
217 required concentration. The required dose of dofetilide was obtained by serial dilution. We chose
218 to use 0.3 μM because the dofetilide hERG IC_{50} value is <10 nM which, assuming a Hill coefficient
219 of one, should correspond to $>97\%$ conductance block of I_{Kr} at 0.3 μM dofetilide. We avoided
220 higher concentrations as dofetilide does have other known voltage-dependent ion channel targets
221 whose IC_{50} s are in the 10s–100s of μM range (Mirams et al., 2011). Between the two recordings we
222 allowed the dofetilide-induced current block to reach equilibrium (under Pr0). We then subtracted
223 the currents that remained in the presence of dofetilide from those recorded in the presence of
224 vehicle to remove any contribution of endogenous currents (and to produce what we refer to as
225 ‘dofetilide subtracted’ data). Prior to performing this subtraction, we first leak subtracted both the
226 vehicle and dofetilide recordings individually, as described above. It may not always be necessary for
227 dofetilide subtraction to be performed on CHO cells, as endogenous voltage-dependent currents can
228 be very low, and leak subtraction may suffice (see Appendix B1.6). But we applied the dofetilide
229 subtraction method nonetheless to generate a gold-standard dataset for this study.

230 2.4 Mathematical Model

231 Whilst our model is equivalent to a two gate Hodgkin-Huxley formulation, we use a Markov model
232 description in practice (simply to generalise the computational code for other model structures;
233 the relationship between equivalent Markov and Hodgkin-Huxley models is explained in Keener
234 and Sneyd (2009), vol. 1, p150). The system of ordinary differential equations underlying the
235 mathematical model structure shown in Figure 4B is then:

$$\frac{dC}{dt} = -(k_1 + k_3)C + k_2O + k_4[IC], \quad (3)$$

$$\frac{dO}{dt} = -(k_2 + k_3)O + k_1C + k_4I, \quad (4)$$

$$\frac{dI}{dt} = -(k_2 + k_4)I + k_3O + k_1[IC], \quad (5)$$

236 where the fourth state is constrained by probabilities of state occupancies summing to one

$$[IC] = 1 - (C + O + I). \quad (6)$$

237 The eight parameters P_1 to P_8 determine the rates k_1 to k_4 according to the exponential voltage-
238 dependence relationships shown in Figure 4B. The current, I_{Kr} , is modelled with a standard Ohmic
239 expression:

$$I_{\text{Kr}} = G_{\text{Kr}}O(V - E_K), \quad (7)$$

240 where G_{Kr} is the maximal conductance, E_K is the Nernst potential for potassium ions, and O is the
241 open probability, given by the solution to the system of equations above. E_K is not inferred, but
242 is calculated directly from the ratio of ion concentrations on each side of the cell membrane using
243 the Nernst equation:

$$E_K = \frac{RT}{zF} \ln \left(\frac{[K]_{\text{out}}}{[K]_{\text{in}}} \right). \quad (8)$$

244 where R is the ideal gas constant, T is the temperature, F is the Faraday constant, z is the valency
245 of the ions (in this case 1), and $[K]$ represents the concentration of potassium ions. Note that this
246 expression has a temperature dependence, and the temperature of the bath was recorded for each
247 cell and used in relevant simulations.

248 All simulations were performed in MatLab. Mex functions were used to define the equations and
249 simulate by using CVODE (Hindmarsh et al., 2005) to solve the systems of differential equations,
250 with both absolute and relative tolerances set to 10^{-8} . Code is available to download as described
251 at the end of the manuscript.

252 2.5 Parameter Inference

253 We used a global minimisation algorithm (Hansen et al., 2003) followed by a custom-written
254 Bayesian inference method. Parameters were estimated using a Monte Carlo based inference scheme,
255 in this case using an approach similar to that described in Johnstone et al. (2016). In Appendix B2
256 we give details of how: (1) a likelihood is assigned to any candidate parameter set; (2) maximising
257 the likelihood using a global optimisation scheme gives a ‘best fit’ parameter set; (3) uniform prior
258 distributions are assigned to the kinetic parameters; and (4) we start a Markov chain Bayesian
259 inference scheme from the estimated global optimum to generate a posterior probability distribu-
260 tion. The benefits of this scheme are that we explore the ‘parameter space’ widely and build up a
261 probability distribution (probability of parameters generating the experimental results we observed)
262 across the whole parameter space, thereby characterising any uncertainty in the ‘best fit’ parameter
263 set. This posterior distribution allows us to check that we are constraining each parameter’s value
264 with the information in the experiment, and are not experiencing problems with identifiability of
265 parameters (Siekmann et al., 2012).

266 2.6 Note on Normalisation

267 Where existing literature model simulations were plotted alongside experimental traces, or one
268 experimental trace was compared with another, we first had to normalise to account for differences
269 in conductance values. This was achieved by selecting a scaling factor for the conductance value for
270 each model simulation (or experimental trace) that minimised the square difference between each
271 trace and a reference experimental trace.

272 For literature models the reference trace was the experimental current from the action potential
273 clamp Pr6. Note this provides a best-case fit to Pr6 for all of the literature models, removing the
274 possibility that some models open ‘half as much’ because they have ‘twice the conductance’. For the
275 new model, no scaling was applied and conductance was directly fitted to the experimental current
276 from the sinusoidal protocol (along with other parameters).

277 3 Results

278 3.1 Model Calibration

279 We calibrate a mathematical model using only data recorded under the sinusoidal protocol (Pr7).
280 The Hodgkin and Huxley-style structure of the model we use, and its corresponding model param-
281 eters, can be seen in Figure 4B. We independently fitted this model to each of the experimental
282 current traces shown in Figure 3. For each cell, we obtain a probability distribution of estimates for
283 each parameter that captures any observational uncertainty in the parameter values (Pathmanathan
284 and Gray, 2013; Mirams et al., 2016).

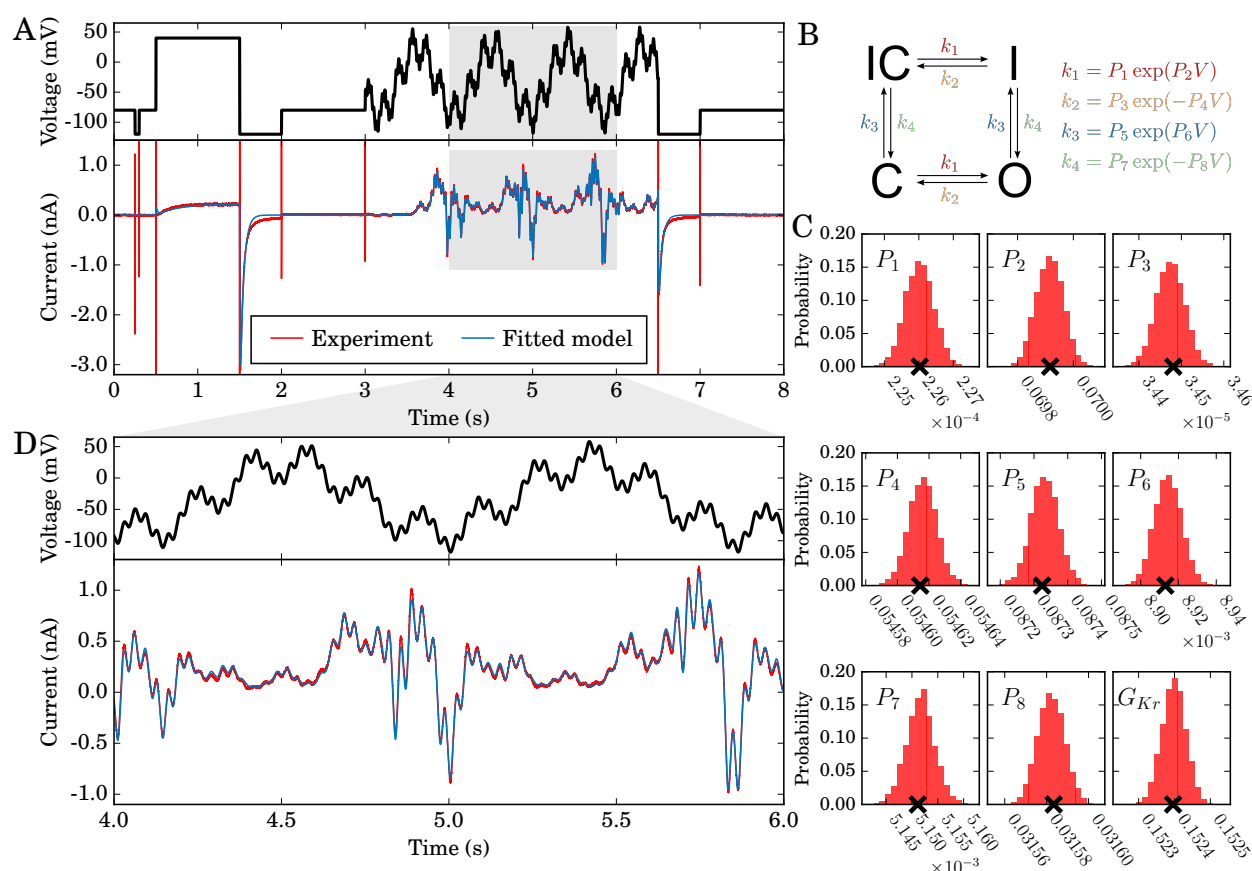


Figure 4: **Model calibration.** **A:** Top: the entire 8 second training protocol, bottom: an experimental recording with the fitted model simulation overlaid (portion of the sinusoid enlarged in panel D). This simulation uses the maximum posterior density parameter set, denoted with crosses in panel C. **B:** The model structure in Markov state diagram format, note that the symmetric transition rates mean this is equivalent to a Hodgkin and Huxley-style model with two independent gates. Parameter values P_1 to P_8 define voltage (V)-dependent transitions (k) between conformational states. **C:** posterior distribution of single-cell derived model parameters. Probability density distributions are shown for each parameter after fitting to the experimental data shown in panel A. The parameter numbering corresponds to that shown in panel B. Crosses indicate the parameter set with the maximum posterior density. The standard deviation of each of these distributions is less than 0.2% of the maximum posterior density value. **D:** an enlargement of the highlighted region of panel A.

285 The result of the fitting procedure for one cell is shown in Figure 4. The parameter set with
 286 maximum posterior density is shown in Figure 4A, demonstrating an excellent fit between experi-
 287 mental and simulated data. The resulting posterior probability density for the parameters obtained
 288 from this Bayesian inference approach is projected across each parameter in Figure 4C. We also
 289 tested that our approach is theoretically appropriate for inferring all parameters by using synthetic
 290 data studies, as described in Appendix C. The plausible parameter space is very narrow: if multiple
 291 parameter set samples are taken from the distribution shown in Figure 4C, the resulting simulated
 292 current traces are indistinguishable to the eye. To quantify this, taking 1000 samples we find that
 293 the 95% credible intervals for the simulated currents were always within at most either 3.47% or,

294 in absolute terms, 0.0043 nA of the simulated current given by the maximum posterior density
295 parameter set.

296 The results we present in Figure 4 are from a single cell with a good quality recording and a
297 high signal:noise ratio (this choice of cell, and other cells' predictions, are discussed later). We
298 fit models on a cell-specific basis, and then also use averaged experimental data to create a single
299 'averaged' model as described in Appendix F. We will compare these approaches below. We provide
300 all parameter values with the maximum posterior density for all models in Appendix Table F11.

301 3.2 Validation predictions

302 Having trained our model to eight seconds of experimental data from the sinusoidal protocol Pr7,
303 we now test its ability to predict more than 5 minutes of independent experimental behaviour.
304 We predict the current in response to traditional voltage-step protocols Pr1–5 (adapted from those
305 previously used in the literature (Bett et al., 2011)), and also to a novel physiologically-inspired
306 voltage clamp protocol comprised of multiple action potentials (Pr6). All recordings shown in
307 Figures 4–6 are from the same cell, using the experimental procedure shown in Figure 2.

308 To make the predictions for Protocols Pr1–6 we performed simulations using the parameter
309 set with the maximum posterior density in the fit to the sinusoidal protocol (Pr7). As with the
310 calibration protocol, all the predictions we will discuss below are indistinguishable by eye from the
311 result of taking multiple samples from the distributions in Figure 4C and plotting a prediction for
312 each of these parameter sets.

313 In Figure 5, we show traditional voltage step protocols, experimental recordings and the simu-
314 lated predictions from the model. We also present some of the most commonly-plotted summary
315 curves for experimental data under these protocols, together with predicted summary curves from
316 our model. We compare these results with the summary curve predictions from a sample of widely-
317 used literature models. We chose models for hERG1a expression systems at room temperature
318 (Wang et al., 1997; Di Veroli et al., 2013) and physiological temperature (Mazhari et al., 2001);
319 and also models with the same Hodgkin-Huxley structure as ours (Zeng et al., 1995; Ten Tusscher
320 et al., 2004) albeit for physiological temperatures, as these are most directly comparable (methods
321 used to derive summary plots are given in Appendix B1.7 with some additional summary curves
322 for Pr1, 2 & 4 in E). We can predict a wide range of current behaviour in response to the standard
323 voltage-step protocols, without having used any of this information to fit the model.

324 There are a number of points to draw attention to in Figure 5. Firstly, most of the current-
325 voltage relationships and time constant-voltage relationships we predict in response to the tradi-
326 tional voltage-step protocols are closer to the experimental data than similar model-experiment
327 comparisons in the literature (even when existing literature models, with more parameters, were
328 fitted to such data). Secondly, there are some weaknesses to the new model — particularly in
329 predictions of the Pr4 summary plot of time constant (τ) of inactivation against voltage, where we
330 predict a time constant that is approximately 4 ms too fast at -40 mV. Yet, it is worth noting that
331 this may be the best fit that is possible with a Hodgkin-Huxley style model: the Ten Tusscher and
332 Zeng models predict timecourses that are so different it is difficult to fit comparable time constants.
333 The current timecourse for Pr4 is actually predicted more accurately than any of the other models
334 shown here (see Appendix Table D6) despite the τ -V relationship being less accurate; in agreement
335 with this, other summary IV curves of Pr4 are predicted more accurately by the new model (see
336 Appendix Figures E9 & E10).

337 Figure 6 shows the model prediction of the currents invoked in response to the physiologically-
338 inspired action potential protocol Pr6, compared with the experimental recording (as shown in
339 Figure 2 we used the first repeat of Pr6 for validation purposes, and the second as a quality control

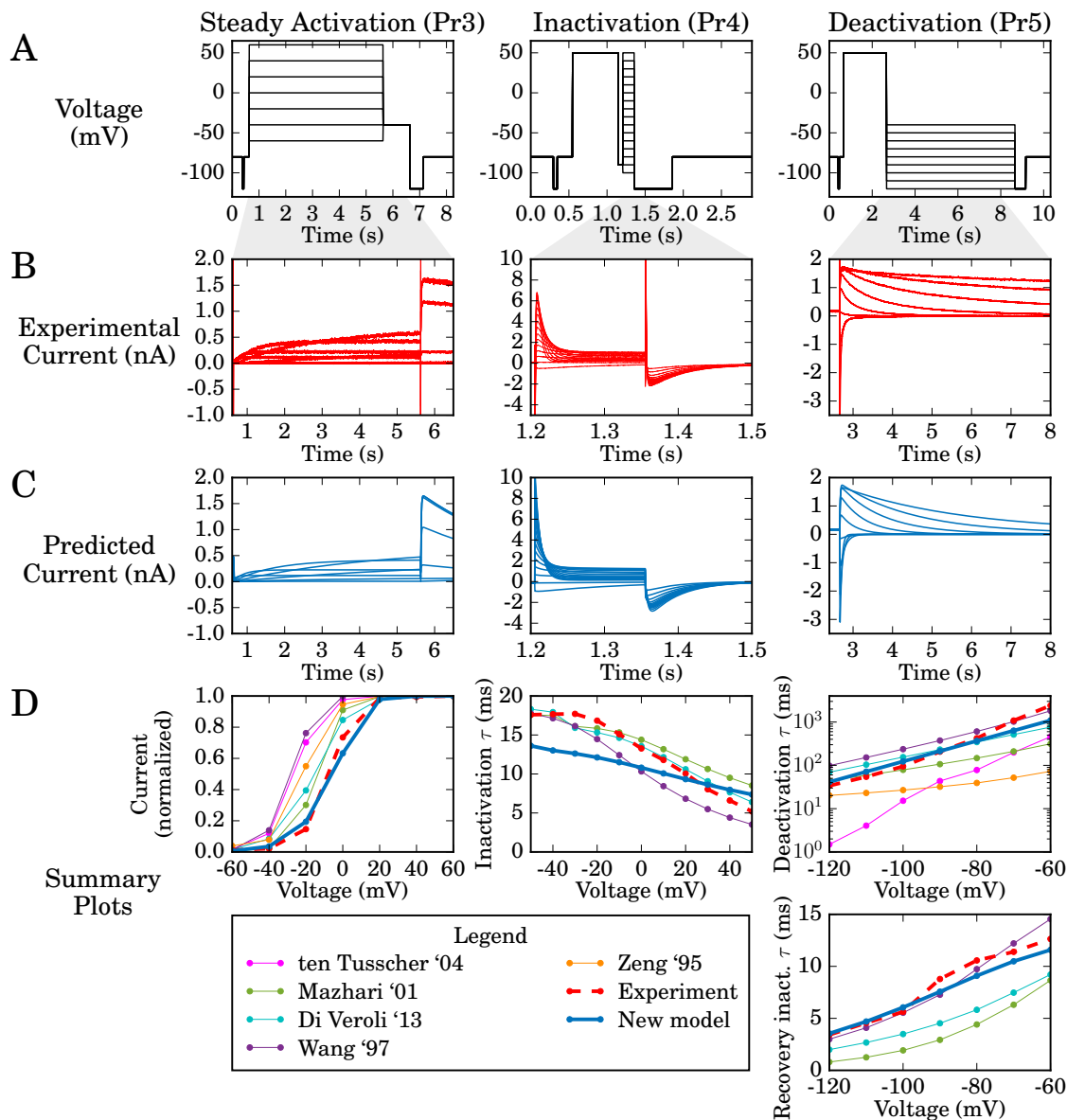


Figure 5: **Validation predictions — currents in response to traditional voltage step protocols.** Each column of graphs corresponds to a validation step protocol: those commonly used to study steady state activation, inactivation and deactivation (Pr3, Pr4, Pr5 in Fig 3) respectively. **A:** the voltage protocols. **B:** experimental current traces. **C:** model response — all are predictions using the maximum posterior density parameter set indicated in Fig 4C calibrated to just the sinusoidal protocol. **D:** summary curves, either current–voltage (I–V) or time constant–voltage (τ –V) relationships. These plots summarise the results in the relevant column. The model prediction is shown in blue bold throughout, and the experimental recording with a dashed red line. Note that the deactivation time constant we plot here is a weighted tau, described in Methods B1.7. Note that some literature model predictions are missing from the summary plots as we were either unable to fit exponential curves to ‘flat’ simulation output reliably; or the exponential decay occurred in the opposite direction to experimental traces, and we considered the comparison unwarranted.

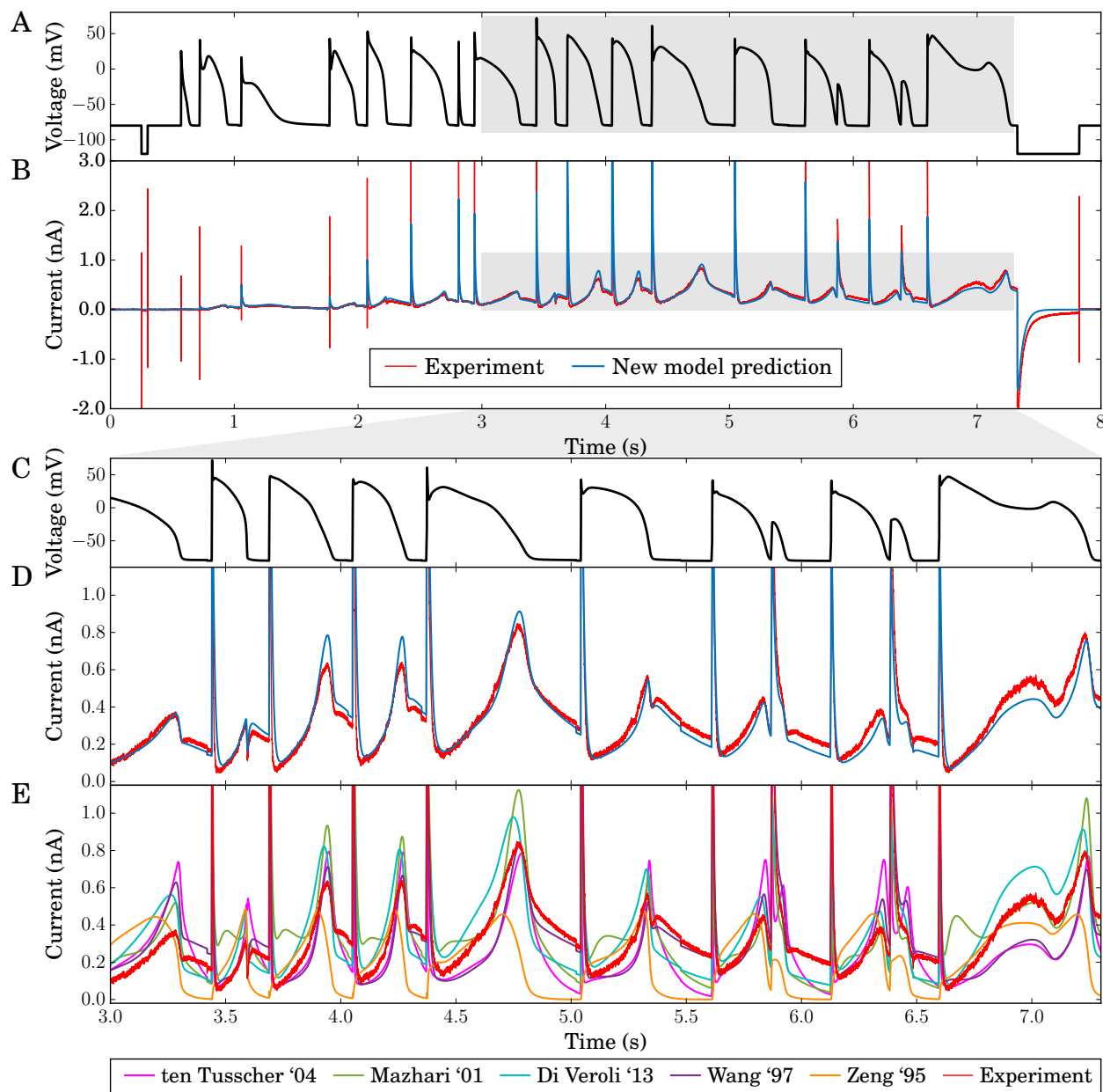


Figure 6: **Validation prediction — the current in response to the action potential protocol.** **A:** the voltage clamp protocol. **B:** a comparison of the experimental recording (red) and new model prediction (blue). **C & D:** enlargements of the highlighted regions of panels A & B. **E:** the same view of the experimental data in panel D, but here compared with predictions from literature I_{K_r} models. Conductance, G_{K_r} , is scaled for each of the literature models to give the least square difference between their prediction and these experimental data, i.e. we display a best-case scaling for each of these models. A quantification of the error in our model prediction versus these literature models is given in Appendix Table D6: the performance shown in panels D and E holds for the whole trace, so the mean error in predicted current across the whole protocol is between 69% and 264% larger for the literature models' predictions than for our sine-wave fitted model.

340 measure). Replicating behaviour under action potentials is perhaps the most important requirement
341 for a hERG channel model for use in physiological or pharmacological studies. The model is able to
342 predict the response to all of the complex action potential protocol extremely well, and much better
343 than existing models (even though we have scaled all the literature models' maximal conductances
344 (G_{K_r}) to fit this trace as well as possible in Figure 6).

345 We provide a quantitative comparison of predicted current traces for our model and each of the
346 literature models for Pr3–7 in Appendix Table D6. In each case, the worst-performing literature
347 model is a Hodgkin-Huxley style model. Yet our simple model, with the same structure, is able
348 to provide significantly better predictions than even the Markov-type models, which are usually
349 considered to be better representations of hERG kinetics (Bett et al., 2011). Our methodology has
350 resulted in a simple and highly predictive mathematical model, able to describe a wide range of
351 physiologically-relevant behaviour.

352 3.2.1 Cell-specific validation

353 In Figure 7A we present the maximum posterior density parameter values when repeating the above
354 approach using data from nine different cells. The clustered parameter values demonstrate that
355 parameters derived from different cells take similar values, giving us confidence that the procedure is
356 reproducible and biophysically meaningful. There is more cell-to-cell variability in some parameters
357 than others, which may be related to variability in the underlying physiological processes that
358 they represent; supporting the value, and perhaps necessity, of a cell-specific approach. We also
359 acknowledge that some parameters may be more or less sensitive to variability in experimental
360 conditions such as temperature, residual background/endogenous currents, and imperfect dofetilide
361 and/or leak subtraction.

362 We order the cells in Figure 7 based on the lowest to highest difference in leak resistance between
363 the vehicle and dofetilide recordings of Pr7. This ordering gives a measure of recording stability, and
364 is intended to be a surrogate for data quality. The cell presented above, in Figures 4–6, corresponds
365 to Cell #5 of 9 under this ranking, so we obtain very good predictions even with our 'median' quality
366 data. We show cell-specific predictions of the current-voltage relationship for the peak steady-state
367 activation current for each cell-specific model in Figure 7B. While we focused on Cell #5 in the
368 results section, Cells #1–4 also produce excellent cell-specific predictions (similar comparisons for
369 other summary plots are in Appendix Figures F12–F14).

370 We also investigated the benefit of our cell-specific approach by building a model using averaged
371 experimental data from all nine cells instead. We describe this approach in Appendix F, and
372 summarise the results in Appendix Table F12. Generally, for the cells with the highest data quality
373 (Cells #1–5) the cell-specific models provide better predictions than the average model, as we see
374 for Pr3 when comparing coloured cell-specific predictions and experiment with the black line for the
375 average model in Figure 7B. The same trend holds for the action potential protocol Pr6, in 8/9 cells
376 the cell-specific model provides less error than the average cell model — the largest improvement
377 was 50% less error; for the remaining cell where the average cell model provided better predictions,
378 this was by 3%.

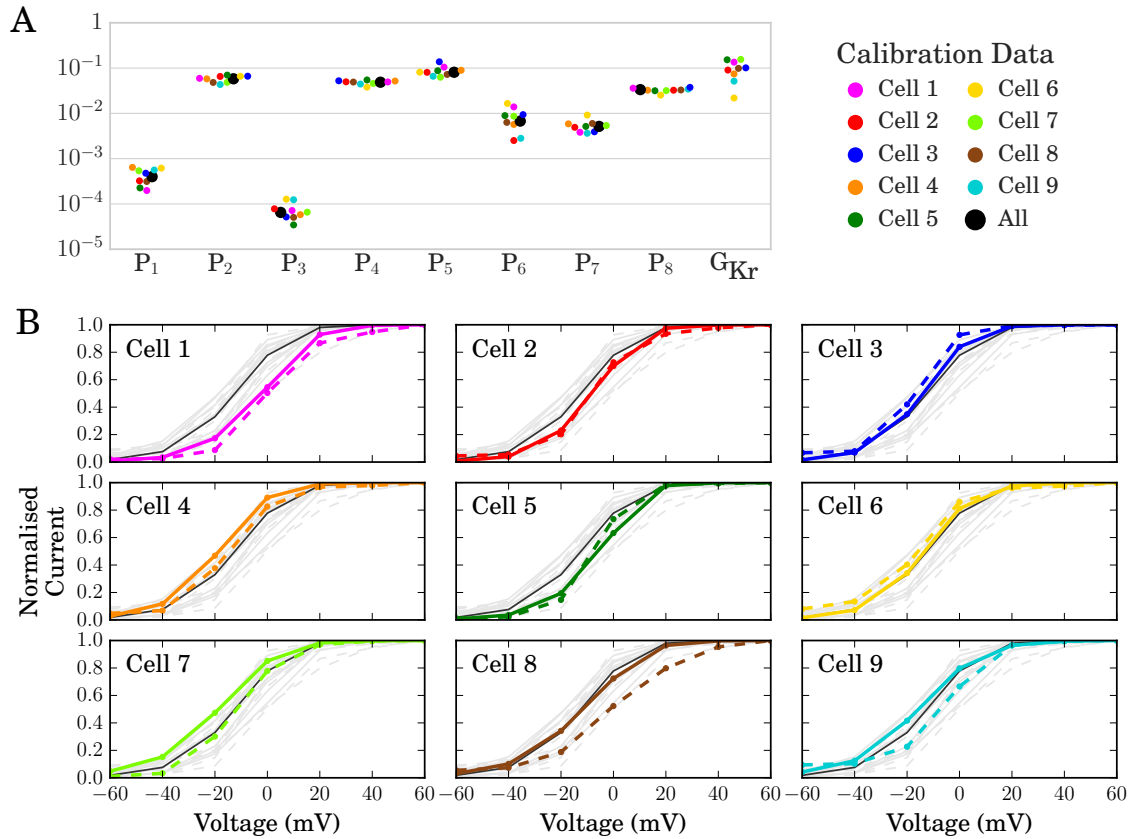


Figure 7: **Cell-specific model parameters, and comparison of their predictions with cell-specific experimental results.** (A:) Plot of parameters (maximum posterior density values) for nine cells obtained from training the model to the sinusoidal voltage protocol recorded on nine different cells, together with parameters calibrated to average data (N.B. not the average of the cell-specific parameters). The full set of parameter values are shown in Appendix Table F11 and the distributions for each parameter shown in Fig F11. (B:) Comparison of cell-specific model predictions to cell-specific experimental recordings for the steady-state peak current I-V curves from Pr3. Each plot represents a different cell, model predictions are depicted by a bold coloured line, and dashed lines show values derived from the experimental data. The black lines (same on each plot) represent the prediction from the model calibrated to averaged sinusoidal data (all of the cells' data). Each subplot contains all of the other cells' recordings and predictions in light grey in the background to aid comparison and show the spread that we observed.

379 4 Discussion

380 In this paper we have presented a novel method for capturing ion current properties, based on
381 constructing mathematical models of ion channel kinetics. We used a sinusoidal voltage protocol to
382 construct a simple model of hERG channel kinetics using just 8 seconds of recording, as opposed to
383 a traditional approach that requires several minutes of voltage-step data. All of our experimental
384 data can be collected from a single cell; whereas traditional protocols require long experiments,
385 and typically require different gating processes to be studied in different experiments in different
386 cells. In future, our approach opens up the possibility of making multiple interventions (such as the
387 addition of drug compounds) since we could re-measure the full ion channel kinetics multiple times
388 in a single cell.

389 The conceptual shift is that channel kinetics should be summarised by mathematical model
390 parameters, not a series of current-voltage (IV) and time constant-voltage curves. In essence, the
391 model *is* the current characterisation, rather than something designed to fit IV and time constant
392 curves, which only represent a certain subset of possible behaviours of the current. The success of
393 the approach lies in moving away from traditional protocols that can be easily interpreted by eye,
394 which typically require the current to return to an equilibrium rest state between voltage steps.
395 Instead, our protocol also probes non-equilibrium ion channel behaviour by rapidly exploring time
396 and voltage dependence, and is interpreted through the fitting of a model for the whole current at
397 once.

398 Our model is able to replicate the experimental training data very well (Fig 4). This is often
399 the point at which traditional approaches in the literature have stopped, and concluded that a
400 mathematical model is a good representation of ion channel kinetics (also true more generally
401 for mathematical models of biological processes). Instead, we performed an extremely thorough
402 evaluation of the model by testing its ability to predict the behaviour in response to a series of
403 voltage clamp protocols it has not ‘seen before’ (both those traditionally used to characterise hERG
404 channel kinetics, and also a new complicated series of action potential waveforms), all recorded
405 from the same cell as the training data. We are not aware of such a thorough, physiologically-
406 relevant validation of an ion channel model having been performed before. Testing that we are
407 able to predict the current response to a voltage pattern which may be observed in physiological
408 or patho-physiological conditions is a particularly robust and useful way to validate a model, and
409 critical if an I_{Kr} model is to be used to accurately predict cardiac electrical activity in both healthy
410 and potentially arrhythmic situations.

411 The extremely good prediction from all our cell-specific models of the response to the complex
412 action potential protocol is particularly remarkable (Fig 6). Cell-to-cell variability in ion channel
413 kinetics was captured by fitting different underlying kinetic parameters. These parameter sets were
414 shown to have modest variation, and this variation in kinetics was quantitatively predictive of
415 variation observed in independent validation experiments (Fig 7).

416 Cell-specific predictions were particularly strong when using the highest quality data, high-
417 lighting the necessary data quality for constructing accurate and robust models of ion channel
418 kinetics. The cell-specific models outperformed a model constructed using averaged data from mul-
419 tiple cells/experiments, in line with the ‘failure of averaging’ discussed in Golowasch et al. (2002)
420 and the problems of fitting to averaged summary curves outlined in Pathmanathan et al. (2015).

421 Our inactivation protocol (Pr4) showed that it is possible for models to fit some (or all) summary
422 curves well, without necessarily replicating the underlying current traces with less error. Often
423 studies present just single summary curves in isolation. But we have seen how models can fit
424 certain summary curves well, whilst fitting others badly. Models that have less accurate summary
425 curves may even predict the underlying current traces more reliably; and, importantly, vice-versa.

426 A focus on these summary curves to represent kinetics and fit mathematical model behaviour was
427 necessary in the era of hand fitting parameters using graph paper, but should perhaps now be
428 superseded by fitting/comparing directly to experimental current traces. By fitting directly, we also
429 reduce the possible influence of subjective choices during time-constant fitting used in the generation
430 of time-constant voltage relationships.

431 A limitation of our study is that our model was trained on experiments performed in expression
432 line cells, creating a hERG1a model at room temperature; compared to native I_{Kr} current in cardiac
433 cells which will have additional isoforms, subunits and regulation at physiological temperatures. As
434 a result, we do not state that this ion current model would necessarily give better performance
435 within a cardiac action potential model. To characterise native I_{Kr} kinetics we plan to apply the
436 methodology presented here in myocytes, to make a model that is more applicable for use in cardiac
437 safety testing and whole-organ simulations. The presence of many larger voltage-dependent currents
438 than we observe in expression systems will make this challenging, but a dofetilide subtraction
439 approach may still yield good results.

440 There are still some aspects of the experimental behaviour that are not replicated by our model.
441 These aspects may be a consequence of using a simple Hodgkin-Huxley style model formulation,
442 although it remains a commonly-used structure for currents within action potential models. In
443 particular, there is only one time constant of deactivation, and low voltage-dependence in the
444 inactivation time constant (Fig 5). A more complicated model with additional states and parameters
445 may be needed to capture certain behaviours.

446 We assessed the capability of the protocol to fit a more complex five state Markov model for
447 hERG (the model proposed by Wang et al., 1997), and show the results in Appendix H. Previously,
448 Bett et al. (2011) explored the behaviours of a subset of existing hERG models and concluded that
449 this model was best able to replicate activation kinetics. In Appendix H we show that exactly
450 the same approach and algorithms again tightly constrained all 15 of the parameters in this larger
451 model, using the same sinusoidal protocol data. The more complex model resulted in a better fit
452 to the calibration data, and also made good predictions for the validation protocols — although
453 not quite as good as the simpler model presented here in the main text. This finding highlights the
454 importance and challenges of selecting the most appropriate level of complexity for a mathematical
455 model.

456 So despite our simple model not replicating precisely the full range of behaviour, neither do the
457 existing, more complex, models available in the literature. We have shown that our simple model
458 can provide better predictions than the literature models for all the raw current timecourses, if not
459 all summary curves, in the majority of cells. In fact, the simplicity of our model may be the key to
460 its success — with only eight kinetic parameters we have confidence that they are all being fitted
461 well, and we have shown that there is low uncertainty in their values.

462 The applicability of our approach for different ion channels will be heavily dependent on the
463 precise form of the sinusoidal protocol that is used, and in parallel work we are developing different
464 strategies for optimising the voltage protocol design for given currents. Although we have also shown
465 that the existing protocol is at least theoretically appropriate for parameterising an I_{Ks} model in
466 Appendix G. In future work, ideas from control engineering may be useful. Seemingly unconnected
467 problems, such as generating signals to characterise the state of lithium ion batteries (Xiong et al.,
468 2011), are in fact very similar mathematical challenges.

469 There will be limits in the complexity of model structure and number of parameters that any
470 protocol can constrain. But in terms of limitations of this style of protocol, we consider that
471 the more information-rich protocols are, the better; and these new protocols may enable us to
472 accurately calibrate larger models than before. We strongly advocate synthetic data studies to
473 assess the suitability of a given protocol for constraining parameters of a given model — seeing

474 whether re-fitting to data generated by simulations of your model and protocol can recover the
475 parameters used in the simulation. Such approaches are necessary but not sufficient: they still rely
476 on the models being a good representation of the system under study, and incorporating statistical
477 ideas to handle model discrepancy (the difference between models and reality) is an important line of
478 enquiry (Strong et al., 2012). In other parallel work, we are extending the approach presented here
479 for selecting between different possible model structures for hERG channel kinetics (see Appendix
480 Fig A1 for the range of possibilities; and Kargol (2013) for an outline of how this may be approached
481 by optimising the protocols themselves to assist with this task).

482 Considering probabilistic uncertainty in model parameters and predictions is evermore important
483 as models begin to be used for safety-critical predictions (Pathmanathan and Gray, 2013; Mirams
484 et al., 2016). These predictions include guiding therapies (Arevalo et al., 2016) and pharmaceutical
485 safety assessment with the Comprehensive in-vitro Proarrhythmia Assay initiative being pursued by
486 the FDA in collaboration with industry, academia and other regulators (Sager et al., 2014; Fermini
487 et al., 2016). Here we have shown there is very low uncertainty in hERG kinetics parameters in a
488 single cell, and also characterised the variability in these estimates between different cells.

489 In summary, we have demonstrated significant advantages in our cell-specific mathematical
490 modelling approach, observing excellent model predictions of currents in response to protocols the
491 model was not trained to replicate. The simple ion channel state arrangement we have assumed
492 must capture the most important features underlying hERG state transitions, despite being much
493 simpler than many previous models in the literature. The information-rich approach allows, for
494 perhaps the first time, an exploration of both within-cell and between-cell variability in ion channel
495 kinetics. The significant time saving of our short protocol also leads to datasets that are more
496 consistent and therefore of higher quality, since little changes in experimental conditions during
497 the 8 second recording interval. Its brevity opens up the possibility of taking more recordings in
498 different experimental conditions within a single cell (e.g. drug concentrations (Pearlstein et al.,
499 2016; Lee et al., 2016) or temperatures (Vandenberg et al., 2006)). These datasets will result in
500 more accurate descriptions of ionic currents in these different conditions in the heart and other
501 organ systems.

502 Acknowledgements

503 Our thanks to Prof. Gail Robertson of University of Wisconsin–Madison for assistance in acquiring
504 the cell line used in pilot stages of this study. We would also like to thank the following people for
505 technical assistance, access to facilities, support and encouragement: Jim Louttit, Nick McMahon,
506 Carol Wilson, Sam Turner, Kate Harris and Sara Graham of GSK Safety Assessment; Jules Hancox
507 of University of Bristol; Monique Windley and Mark Hunter of Victor Chang Cardiac Research
508 Institute; Rianne Rijken and Birgit Goversen of UMC Utrecht. Thanks to Ross Johnstone (Uni-
509 versity of Oxford) for removing singularities from the Zeng model, and to Frank Ball (University of
510 Nottingham) for comments on a paper draft.

511 Funding

512 KAB was supported by the EPSRC and GlaxoSmithKline Plc (grant numbers EP/G037280/1,
513 EP/I017909/1 and EP/K503769/1). JIV and APH acknowledge funding from the NHMRC. RB
514 acknowledges support from ANR grant BoB ANR-16-CE23-0003. GRM gratefully acknowledges
515 support from a Sir Henry Dale Fellowship jointly funded by the Wellcome Trust and the Royal
516 Society (grant number 101222/Z/13/Z).

517 Author Contributions

518 KAB, RB, YC, DJG, TdeB, GRM designed the study and modelling approach; KAB, RB & GRM
519 designed and implemented the statistical methods; KAB, GRM, JIV, APH and TdeB designed and
520 refined the experimental methods; KAB performed all the experiments, simulations and statistical
521 analysis; KAB, TdeB, GRM wrote the manuscript; all authors approved the final version of the
522 manuscript.

523 Competing Interests

524 The authors declare that the research was conducted in the absence of any commercial or financial
525 relationships that could be construed as a potential conflict of interest. The opinions presented here
526 are those of the authors. No official support or endorsement by the Food & Drug Administration
527 is intended nor should be inferred.

528 Materials

529 All computational codes, and the experimental current recordings that were used for calibration and
530 validation (leak and dofetilide subtracted), are openly available in a Supplementary Data reposi-
531 tory at <https://github.com/mirams/sine-wave>. A permanently archived version is available on
532 Figshare at <https://doi.org/10.6084/m9.figshare.4704550.v5> alongside the full raw data (in
533 both plain text and pClamp formats) at <https://doi.org/10.6084/m9.figshare.4702546.v1>.

534 For additional details on the methods please see the online Appendix.

535 References

- 536 Arevalo HJ, Vadakkumpadan F, Guallar E, Jebb A, Malamas P, Wu KC & Trayanova NA (2016).
537 Arrhythmia risk stratification of patients after myocardial infarction using personalized heart
538 models. *Nature Communications* **7**, 11437.
- 539 Babcock JJ & Li M (2013). hERG channel function: beyond long QT. *Acta Pharmacologica*
540 *Sinica* **34**, 329–35.
- 541 Balsler JR, Roden DM & Bennett PB (1990). Global parameter optimization for cardiac potassium
542 channel gating models. *Biophysical Journal* **57**, 433–44.
- 543 Bett GC, Zhou Q & Rasmusson RL (2011). Models of HERG Gating. *Biophysical Journal* **101**,
544 631–642.
- 545 Cannon RC & D’Alessandro G (2006). The ion channel inverse problem: neuroinformatics meets
546 biophysics. *PLoS Comput Biol* **2**, e91.
- 547 Cooper J, Scharm M & Mirams GR (2016). The cardiac electrophysiology web lab. *Biophysical*
548 *Journal* **110**, 292–300.
- 549 Di Veroli G, Davies M, Zhang H, Abi-Gerges N & Boyett M (2013). High-throughput screening of
550 drug-binding dynamics to HERG improves early drug safety assessment. *American Journal of*
551 *Physiology-Heart and Circulatory Physiology* **304**, H104–H117.

- 552 Farrelly AM, Ro S, Callaghan BP, Khoyi MA, Fleming N, Horowitz B, Sanders KM & Keef KD
553 (2003). Expression and function of KCNH2 (HERG) in the human jejunum. *American Journal*
554 *of Physiology. Gastrointestinal and Liver Physiology* **284**, G883–95.
- 555 Fermini B, Hancox JC, Abi-Gerges N, Bridgland-Taylor M, Chaudhary KW, Colatsky T, Correll
556 K, Crumb W, Damiano B, Erdemli G, Gintant G, Imredy J, Koerner J, Kramer J, Levesque P,
557 Li Z, Lindqvist A, Obejero-Paz CA, Rampe D, Sawada K, Strauss DG & Vandenberg JI (2016).
558 A New Perspective in the Field of Cardiac Safety Testing through the Comprehensive In Vitro
559 Proarrhythmia Assay Paradigm. *Journal of Biomolecular Screening* **21**, 1–11.
- 560 Fink M & Noble D (2009). Markov models for ion channels: versatility versus identifiability and
561 speed. *Philosophical Transactions of the Royal Society A* **367**, 2161–2179.
- 562 Golowasch J, Goldman MS, Abbott L & Marder E (2002). Failure of averaging in the construction
563 of a conductance-based neuron model. *Journal of Neurophysiology* **87**, 1129–1131.
- 564 Groenendaal W, Ortega FA, Kherlopian AR, Zygmunt AC, Krogh-Madsen T & Christini DJ (2015).
565 Cell-Specific Cardiac Electrophysiology Models. *PLoS Computational Biology* **11**, e1004242.
- 566 Hansen N, Muller S & Koumoutsakos P (2003). Reducing the time complexity of the derandomized
567 evolution strategy with covariance matrix adaptation (CMA-ES). *Evolutionary Computation* **11**,
568 1–18.
- 569 Hindmarsh A, Brown P, Grant K, Lee S, Serban R, Shumaker D & Woodward C (2005). SUNDI-
570 ALS: Suite of nonlinear and differential/algebraic equation solvers. *ACM Trans. Math. Software*
571 *(TOMS)* **31**, 363–396.
- 572 Hobbs KH & Hooper SL (2008). Using complicated, wide dynamic range driving to develop models
573 of single neurons in single recording sessions. *Journal of Neurophysiology* **99**, 1871–1883.
- 574 Hodgkin AL & Huxley AF (1952). A quantitative description of membrane current and its appli-
575 cation to conduction and excitation in nerve. *Journal of Physiology* **117**, 500–544.
- 576 Hosein-Sooklal A & Kargol A (2002). Wavelet analysis of nonequilibrium ionic currents in human
577 heart sodium channel (hh1a). *Journal of Membrane Biology* **188**, 199–212.
- 578 Jehle J, Schweizer PA, Katus HA & Thomas D (2011). Novel roles for hERG K(+) channels in cell
579 proliferation and apoptosis. *Cell Death & Disease* **2**, e193.
- 580 Johnstone RH, Chang ET, Bardenet R, de Boer TP, Gavaghan DJ, Pathmanathan P, Clayton RH
581 & Mirams GR (2016). Uncertainty and variability in models of the cardiac action potential: Can
582 we build trustworthy models? *Journal of Molecular and Cellular Cardiology* **96**, 49–62.
- 583 Kargol A, Hosein-Sooklal A, Constantin L & Przewalski M (2004). Application of oscillating po-
584 tentials to the shaker potassium channel. *General Physiology and Biophysics* **23**, 53–76.
- 585 Kargol A (2013). Wavelet-based protocols for ion channel electrophysiology. *BMC Biophysics* **6**, 3.
- 586 Keener J & Sneyd J (2009). *Mathematical Physiology* Interdisciplinary Applied Mathematics:
587 Mathematical Biology. Springer.

- 588 Lastraioli E, Perrone G, Sette A, Fiore A, Crociani O, Manoli S, D'Amico M, Masselli M, Iorio
589 J, Callea M, Borzomati D, Nappo G, Bartolozzi F, Santini D, Bencini L, Farsi M, Boni L, Di
590 Costanzo F, Schwab A, Onetti Muda A, Coppola R & Arcangeli A (2015). hERG1 channels drive
591 tumour malignancy and may serve as prognostic factor in pancreatic ductal adenocarcinoma.
592 *British Journal of Cancer* **112**, 1076–87.
- 593 Lee W, Mann SA, Windley MJ, Imtiaz MS, Vandenberg JI & Hill AP (2016). In silico assessment
594 of kinetics and state dependent binding properties of drugs causing acquired LQTS. *Progress in*
595 *Biophysics and Molecular Biology* **120**, 89–99.
- 596 Loewe A, Wilhelms M, Schmid J, Krause MJ, Fischer F, Thomas D, Scholz EP, Dössel O & Seemann
597 G (2015). Parameter Estimation of Ion Current Formulations Requires Hybrid Optimization
598 Approach to Be Both Accurate and Reliable. *Frontiers in Bioengineering and Biotechnology* **3**,
599 209.
- 600 Mazhari R, Greenstein J, Winslow R, Marbán E & Nuss H (2001). Molecular interactions between
601 two Long-QT syndrome gene products, HERG and KCNE2, rationalized by in vitro and in silico
602 analysis. *Circulation Research* **89**, 33–38.
- 603 Mirams GR, Cui Y, Sher A, Fink M, Cooper J, Heath B, McMahon N, Gavaghan D & Noble D
604 (2011). Simulation of multiple ion channel block provides improved early prediction of compounds'
605 clinical torsadogenic risk. *Cardiovascular Research* **91**, 53.
- 606 Mirams GR, Pathmanathan P, Gray RA, Challenor P & Clayton RH (2016). White paper: Un-
607 certainty and variability in computational and mathematical models of cardiac physiology. *The*
608 *Journal of Physiology* **594**, 6833–6847.
- 609 Parkington HC, Stevenson J, Tonta MA, Paul J, Butler T, Maiti K, Chan EC, Sheehan PM,
610 Brennecke SP, Coleman HA & Smith R (2014). Diminished hERG K⁺ channel activity facilitates
611 strong human labour contractions but is dysregulated in obese women. *Nature communications* **5**,
612 4108.
- 613 Pathmanathan P & Gray RA (2013). Ensuring reliability of safety-critical clinical applications of
614 computational cardiac models. *Frontiers in Physiology* **4**, 1–9.
- 615 Pathmanathan P, Shotwell MS, Gavaghan DJ, Cordeiro JM & Gray RA (2015). Uncertainty quan-
616 tification of fast sodium current steady-state inactivation for multi-scale models of cardiac elec-
617 trophysiology. *Progress in biophysics and molecular biology* **117**, 4–18.
- 618 Pearlstein RA, MacCannell KA, Erdemli G, Yeola S, Helmlinger G, Hu QY, Farid R, Egan W,
619 Whitebread S, Springer C, Beck J, Wang HR, Maciejewski M, Urban L & Duca JS (2016).
620 Implications of Dynamic Occupancy, Binding Kinetics, and Channel Gating Kinetics for hERG
621 Blocker Safety Assessment and Mitigation. *Current Topics in Medicinal Chemistry* **16**, 1792–818.
- 622 Pollard CE, Abi-Gerges N, Bridgland-Taylor MH, Easter A, Hammond TG & Valentin JP (2010).
623 An introduction to QT interval prolongation and non-clinical approaches to assessing and reducing
624 risk. *British Journal of Pharmacology* **159**, 12–21.
- 625 Redfern W, Carlsson L, Davis A, Lynch W, MacKenzie I, Palethorpe S, Siegl P, Strang I, Sullivan
626 A, Wallis R et al. (2003). Relationships between preclinical cardiac electrophysiology, clinical QT
627 interval prolongation and torsade de pointes for a broad range of drugs: Evidence for a provisional
628 safety margin in drug development. *Cardiovascular Research* **58**, 32.

- 629 Sager P, Gintant G, Turner J, Pettit S & Stockbridge N (2014). Rechannelling the cardiac proarrhyth-
630 mia safety paradigm: a meeting report from the cardiac safety research consortium. *American*
631 *Heart Journal* **167**, 292–300.
- 632 Sanguinetti M, Jiang C, Curran M & Keating M (1995). A mechanistic link between an inherited
633 and an acquired cardiac arrhythmia: HERG encodes the IKr potassium channel. *Cell* **81**, 299–307.
- 634 Siekmann I, Sneyd J & Crampin EJ (2012). MCMC can detect nonidentifiable models. *Biophysical*
635 *Journal* **103**, 2275–86.
- 636 Siekmann I, Wagner LE, Yule D, Fox C, Bryant D, Crampin EJ & Sneyd J (2011). MCMC
637 estimation of Markov models for ion channels. *Biophysical Journal* **100**, 1919–29.
- 638 Strong M, Oakley JE & Chilcott J (2012). Managing structural uncertainty in health economic
639 decision models: a discrepancy approach. *Journal of the Royal Statistical Society: Series C*
640 *(Applied Statistics)* **61**, 25–45.
- 641 Ten Tusscher K, Noble D, Noble P & Panfilov A (2004). A model for human ventricular tissue.
642 *American Journal of Physiology-Heart and Circulatory Physiology* **286**, H1573–H1589.
- 643 Tomaiuolo M, Bertram R, Leng G & Tabak J (2012). Models of Electrical Activity: Calibration
644 and Prediction Testing on the Same Cell. *Biophysical Journal* **103**, 2021–2032.
- 645 Trudeau MC, Warmke JW, Ganetzky B & Robertson GA (1995). HERG, a human inward rectifier
646 in the voltage-gated potassium channel family. *Science* **269**, 92.
- 647 Vandenberg JI, Varghese A, Lu Y, Bursill JA, Mahaut-Smith MP & Huang CLH (2006). Tem-
648 perature dependence of human ether-a-go-go-related gene K⁺ currents. *American Journal of*
649 *Physiology: Cell physiology* **291**, C165–75.
- 650 Vandenberg J, Perry M, Perrin M, Mann S, Ke Y & Hill A (2012). hERG K⁺ channels: Structure,
651 function, and clinical significance. *Physiological Reviews* **92**, 1393–1478.
- 652 Wang S, Liu S, Morales M, Strauss H & Rasmusson R (1997). A quantitative analysis of the activa-
653 tion and inactivation kinetics of HERG expressed in *Xenopus* oocytes. *Journal of Physiology* **502**,
654 45–60.
- 655 Xiong R, He H, Guo H & Ding Y (2011). Modeling for lithium-ion battery used in electric vehicles.
656 *Procedia Engineering* **15**, 2869–2874.
- 657 Zeng J, Laurita KR, Rosenbaum DS & Rudy Y (1995). Two components of the delayed rectifier
658 K⁺ current in ventricular myocytes of the guinea pig type theoretical formulation and their role
659 in repolarization. *Circulation Research* **77**, 140–152.
- 660 Zhou Z, Gong Q, Ye B, Fan Z, Makielski JC, Robertson GA & January CT (1998). Properties of
661 herg channels stably expressed in hek 293 cells studied at physiological temperature. *Biophysical*
662 *Journal* **74**, 230–241.